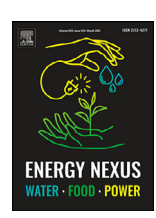


Contents lists available at ScienceDirect

# **Energy Nexus**

journal homepage: www.elsevier.com/locate/nexus



# Design aspects of a fixed focus type Scheffler concentrator and its receiver for its utilization in thermal processing units



Parimal Sharad Bhambare\*, Sudhir Chitrapady Vishweshwara

Department of Mechanical and Industrial Engineering, College of Engineering, National University of Science and Technology, Muscat, Oman

#### ARTICLE INFO

Keywords: Scheffler dish reflector Scheffler concentrator Scheffler receiver Image analysis

# ABSTRACT

Fixed focus type Scheffler concentrators introduced by Wolfgang Scheffler are popularly used for different low to medium industrial process heat applications. These Scheffler concentrators are available in the standard sizes of 8  $\rm m^2$  and 16  $\rm m^2$ . The present paper provides a detailed stepwise procedure for the design of a standing type 16  $\rm m^2$  Scheffler concentrator and its fixed focus receiver, intended to be utilized in a solar thermal processing unit for essential oil distillation at our institute. The dome type receivers of boiler steel grade material, SS-304, are selected for the present application. The diameter of the receiver is estimated based on the analysis of the image formed at the receiver of the Scheffler concentrator. The crossbar equations, seasonal parabola calculations and aperture area calculations for the Scheffler concentrator have also been presented in the paper. The geometrical concentration ratio for the Scheffler reflector dish and receiver system are also evaluated for any given day of the year. The design procedure presented in the paper can be used for designing any suitable size Scheffler concentrator and its receiver as per the energy requirement of the application.

## Introduction

Solar energy is one of the most abundantly available non-conventional energy sources in different tropical regions all over the world. Solar thermal collectors and solar photo voltaic systems are the proven technologies used for harnessing the solar energy for further utilizing it in numerous domestic and industrial applications [44–52] including low to medium capacity power plants [43]. At present fossil fuels are used for meeting the thermal energy requirement of almost all the industrial and domestic applications. The harmful emissions from fossil fuels contributes to the global warming, rising sea water levels and increased acidity of the ocean waters [10]. This alternative utilization of energy from sun in the industries helps in reducing the carbon footprints of the fossil fuels on the environment [10,14].

Scheffler reflectors introduced by Wolfgang Scheffler [20] is an apt solar concentrator technology employed for several low to medium temperature applications in the range of 100 to 200°C [12,14,35,39], to supply the heat energy for their operation [3,4,6,8–10,18,31]. Few of these applications include, thermal desalination [14,15,30], essential oil distillation [12,13,28], bakery [21,24,26], solar cooking [20,22,23,25,29,32,33,38,39], water heating [27,35], crematorium [34], roasting [40], laundry and dry cleaning [36,41]. The basic idea of developing the Scheffler type concentrator was to make solar cooking as comfortable as possible. Scheffler concentrators as compared to

other types solar concentrators are essentially fixed focus type collectors where the focus can be adjusted inside the house or shaded room for cooking purposes as depicted in the following Fig. 1. Scheffler reflector maintains a high-quality focus that requires a simple tracking mechanism and structure so that it can be easily built, maintained and operated in any part of the world [14,15,20,41]. The temperature at the focus of Scheffler concentrator can reach above 200°C. Scheffler concentrators offer several advantages over the other type of solar concentraors. Few of these advantages include, simple construction, simple tracking mechanism, fast installation, lower capital cost, lower operational and maintenance cost, hassle free system in terms of operation, negligible control except seasonal operation and can be operated by the unskilled labors including housewives [14,15,42,53]. Due to these advantages Scheffler concentrators are most suited for the different process heat applications in the rural settings of different parts of the world including Sultanate of Oman [14].

The shape of the Scheffler dish reflector surface is fundamentally a part of the large size parabola, shown by the red colour line in Fig. 1. These concentrators are mostly available in the standard sizes of 8 m² and 16 m² from the manufacturers but can be manufactured up to 50 m² [20]. A few literatures are available for the design of Scheffler concentrators. Munir et al. [11–13], Simone [16] and Anil Kumar et al. [4] has presented the design procedure for the Scheffler concentrators. This design procedure is simple and flexible. Desireddy et al. [5] has developed design charts for the quick estimation of various design parameters for

E-mail address: parimalbhambare@nu.edu.om (P.S. Bhambare).

<sup>\*</sup> Corresponding author.

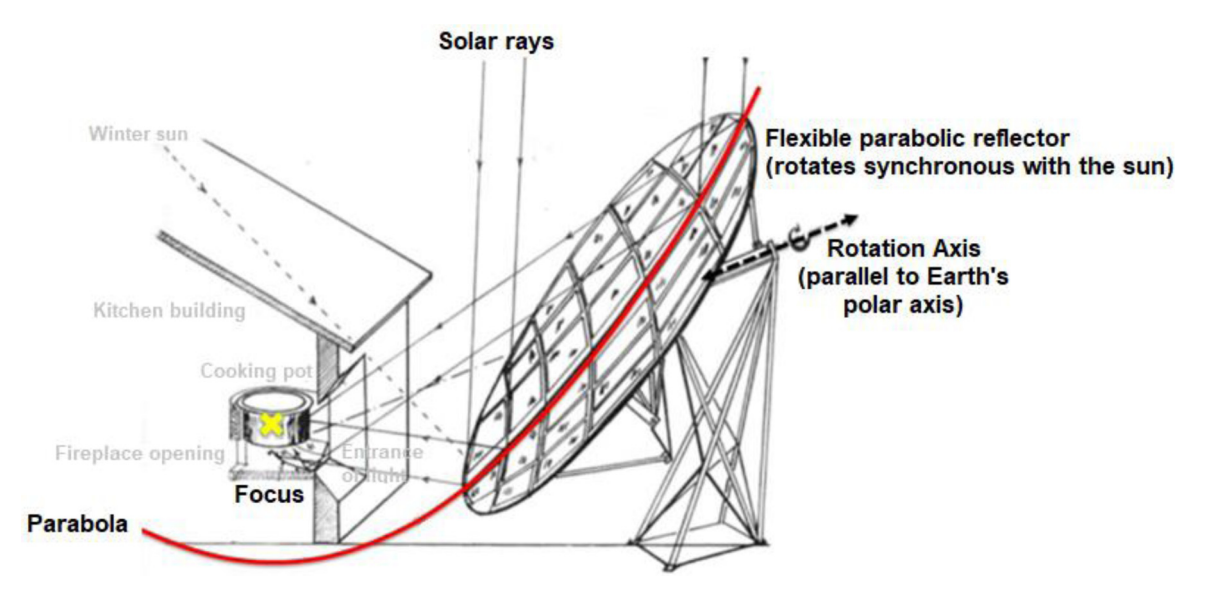


Fig. 1. Graphical representation of Scheffler Concentrator for the solar cooking application [16].

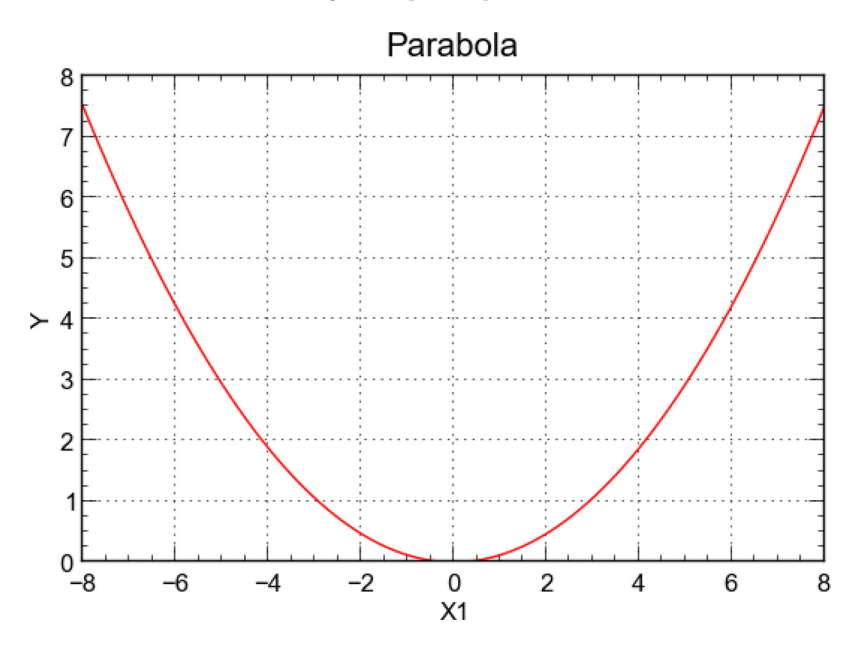


Fig. 2. Basic parabola with vertex at the origin.

the Scheffler concentrators for the manufacturers. Abderrahman et al. [1] has also given a brief review of the design methodologies for Scheffler concentrators.

Although these researchers have provided the guidelines, a detailed stepwise design procedure for the Scheffler reflector is expected. This will certainly help researchers and practicing engineers to develop more applications in this area. This paper presents a detailed stepwise procedure that can be used for designing any size of the Scheffler concentrators along with its dome-type receiver.

# **Design of Scheffler concentrator**

The design of the Scheffler concentrator starts with the calculation of the basic parabola curve for the concentrator. These calculations are done at the equinox (zero solar declination). The vertex of the parabola is considered at the origin as shown below in Fig. 2.

The equation of the parabola with vertex at the origin is given by Eq. (1) below,

$$y = m_n x^2 \tag{1}$$

Here,  $m_p$  is the slope of the parabola. The above parabola when revolved about its y-axis gives the surface of revolution as paraboloid as shown in Fig. 3(i) below. This paraboloid surface needs to be sliced or cut using a cutting plane to define the desired Scheffler dish section as shown in 3-D and 2-D drawings in Fig. 3 below. The slice will create the elliptical rim.

In the 2-D drawing, the slicing plane will be reflected as a straight line that cuts the surface at two points A and B. This is depicted in Fig. 4 below. The line AB is inclined at an angle  $\beta$  to the x-axis. Point C is defined on the parabola such that the tangent passing through it is inclined at 45° to the x-axis. This is required such that the solar radiation at this point will be reflected at 90° and reach horizontally to the focus as shown in Fig. 4 below.

The horizontal ray from point C to the focus (F) forms the daily rotation axis of the reflector during the daily tracking. Point C is kept as close as possible to the centre of the dish to achieve a balanced frame concerning the axis of rotation. When point C is located very close to the center of Gravity of the reflector, the effort required for rotation of the reflector is reduced while minimizing the counterweight required.

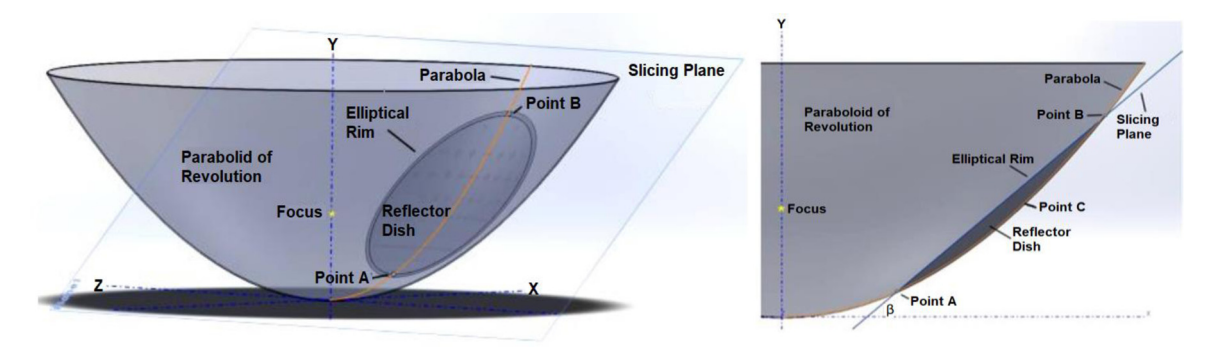


Fig. 3. (i) 3-D view of paraboloid surface with cutting/slicing plane (ii) 2-D view of paraboloid surface with slicing plane [16].

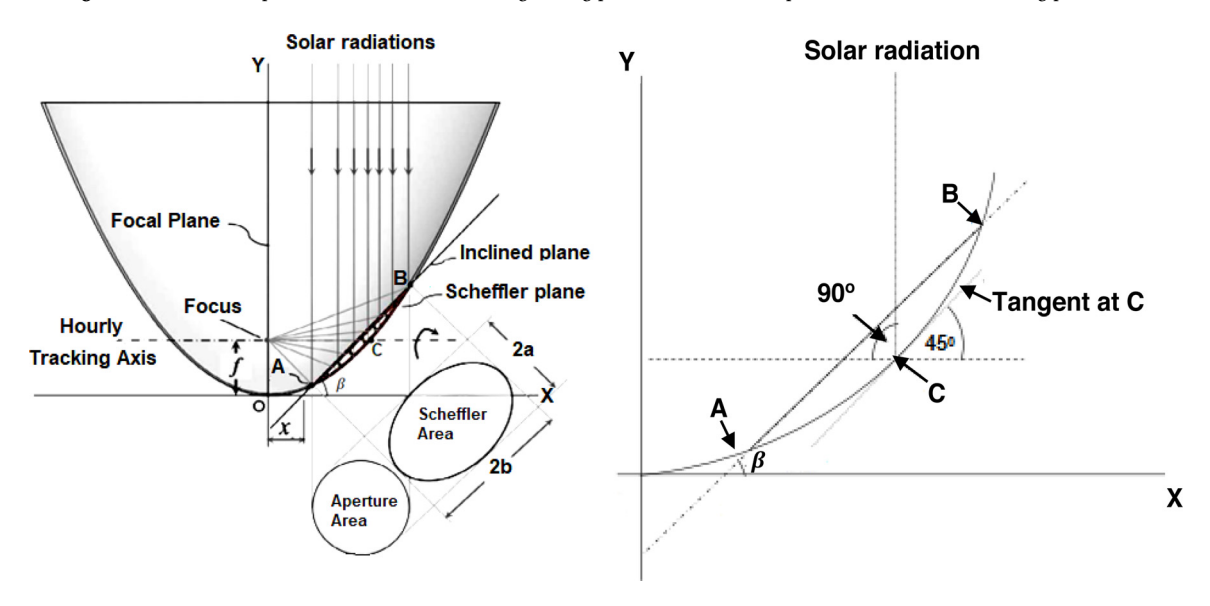


Fig. 4. Scheffler concentrator focusing beam radiations at the focus [5].

Taking the derivative of Eq. (1) to calculate the slope of the parabola,

$$\frac{dy}{dx} = 2m_p x \tag{2}$$

Basic Scheffler concentrator parabola calculations

The basic design of the Scheffler concentrator is initially done with a few simplified considerations. This design is further referred for resizing the concentrator dish to the actual size of  $16\ m^2$ .

The focus height or focal length for a vertical parabola is given as,

$$y_F = \frac{1}{4m_p} \tag{3}$$

Initially, taking the focal length as  $y_F=1$  m. This means the focus is located at a height of 1 m from the vertex of the parabola under consideration. With this, we get the slope,  $m_p=0.25$ . Thus, the parabola equation is,

$$y = 0.25 \ x^2 \tag{4}$$

The x coordinate of C is,  $y_C=2$ . This defines point C completely as, (2, 1). Points A and B are selected as equidistant from C. The distance between these points determines the ratio between the size of the reflector and the distance from the focus. When points A and B are selected farther from each other, the ratio between distance CF and the dish area decreases, this, in turn, increases the curvature of the dish. This makes it easier to focus the solar radiations at the focus while reducing the cost of manufacturing the dish due to losing tolerances.

The angle of inclination  $\beta$  can be varied between 42 and 44.9°. The upper limit is 44.9° due to geometrical constraints. When this angle goes below 41°, the x-intercept of line AB becomes negative. This cast the absorber's shadow on the reflector [5]. For a given focal length increase in inclination,  $\beta$  causes a reduction in aperture area. Based on the literature reviewed this angle is taken as 43.53° for further calculation [5,11,12].

For  $x_A=1$  and  $\beta=43.53^\circ$  the y-coordinate of point A is,  $y_A=0.25$ . This defines point A as (1, 0.25). Now the slope of the line AB is given

$$tan \beta = m_l = \frac{y_B - y_A}{x_B - x_A} \tag{5}$$

For point B, y-coordinate  $y_B$  and the x coordinate,  $x_B$  is calculated as 1.96 and 2.8 respectively. This defines point B completely as (2.8, 1.96). The equation of the line AB can be written as,

$$y_l = m_l x_l + b_l \tag{6}$$

Here,  $m_l$  and  $b_l$  are the slope and y-intercept of line AB. For  $\beta = 43.53^{\circ}$ , the slope and y-intercept of the line is calculated as,

$$m_l = 0.95; b_l = -0.7$$
 (7)

Thus, the final equation of the line AB can be written as,

$$y_l = 0.95 x_l - 0.7 \tag{8}$$

Table 1 below summarizes the final dimensions of the basic Scheffler concentrator dish.

**Table 1**Coordinates of basic Parabola in metre.

Point	X - coordinate	Y - coordinate
A	1	0.25
В	2.8	1.96
C	2	1
F - focus	0	1
Angle $\beta$	43.53°	

**Table 2**Coordinates of revised Parabola in metre.

Point	X - coordinate	Y - coordinate
A	2.135	0.5337
В	5.978	4.1847
С	4.27	2.135
F - focus	0	2.135
Angle $\beta$	43.53°	

# Resizing the Scheffler concentrator parabola

The size of the designed Scheffler is 16 m<sup>2</sup>. The dimensions for the required size Scheffler dish are calculated using the basic parabola as the reference. The coordinates of the basic parabola will be referred to with subscript 1 while for the revised parabola subscript 2 is used. Thus, the equations of these two parabolas are,

$$y_1 = m_1 x_1^2 \text{ and } y_2 = m_2 x_2^2$$
 (9)

The slope  $m_2$  for the modified parabola is calculated using the following relation [16],

$$m_2 = \sqrt{\frac{\pi m_1^2 \left[ \frac{1}{4} \left( x_{B_1} + x_{A_1} \right)^2 - x_{B_1} x_{A_1} \right]}{Area. \cos \left\{ \tan^{-1} \left[ m_1 \left( x_{B_1} + x_{A_1} \right) \right] \right\}}$$
(10)

For Area = 16  $m^2$  and the above coordinates of points  $A_1$  and  $B_1$ , the revised parabola equation is,

$$y_2 = 0.1171x_2^2 \tag{11}$$

The relationships between different coordinates of the basic and the revised parabola are,

$$x_{A_2} = x_{A_1} \frac{m_1}{m_2}; \ x_{B_2} = x_{B_1} \frac{m_1}{m_2}; \ x_{C_2} = \frac{1}{2m_2}$$
 (12)

And,

$$y_{A_2} = y_{A_1} \frac{m_1}{m_2}; y_{B_2} = y_{B_1} \frac{m_1}{m_2}$$
 (13)

The y – coordinate for the focus is calculated using the following equation.

$$y_{F_2} = \frac{1}{4m_2}$$

These coordinates along with coordinates of the focus point, F are summarized in Table 2 below.

For the cutting plane line AB for the revised parabola, the slope now can be calculated as,

$$m_{l_2} = \frac{y_{B_2} - y_{A_2}}{x_{B_2} - x_{A_2}} \tag{14}$$

The revised equation of the cutting plane line AB is obtained as,

$$y = 0.95 \ x - 1.4945 \tag{15}$$

The length of cutting plane line AB represents the major axis of the elliptical frame obtained. This can be calculated as,

$$2b = \sqrt{\left(x_{B_2} - x_{A_2}\right)^2 + \left(y_{B_2} - y_{A_2}\right)^2} \tag{16}$$

For Scheffler dish reflector of area 16 m<sup>2</sup>, the semi-major and semi-minor axes are calculated as b = 2.65 m and a = 1.93 m.

The area of 16 m² is the area of elliptical Scheffler dish that is manufactured further . But as the dish is tilted at 43.53° ( $\approx$  45°), for the incoming sun rays, the projected area or the aperture area as shown in Fig. 4, which is perpendicular to the incoming rays, is the actual area seen by the solar rays and should be considered for the analysis.

The major axis and minor axis of the Scheffler dish are related to each other as shown in Fig. 6. Applying the rules of trigonometry, the aperture area and the dish area are then related to each other by the following relation,

$$\frac{Projected\ Area}{Dish\ area} = \frac{\pi a^2}{\pi ab} = \frac{a}{b} = \cos\ \beta \approx \cos\ (45) = 0.707 \tag{17}$$

From the above discussion, it is clear that the amount of solar radiation captured by the Scheffler dish is about 70% of the actual dish size at the equinox.

The final details of the revised parabola and the Scheffler dish reflector are summarized in Fig. 5.

#### Scheffler crossbar and elliptical frame calculations

Crossbars are used in the elliptical frame to get the required shape of the paraboloid obtained by cutting the plane from the original paraboloid surface. Seven crossbars are distributed equally along the major and minor axes of the parabola with one crossbar at the centre. This section discusses the design and construction of these crossbars and elliptical frames. The equation of the ellipse is,

$$\left(\frac{x}{b}\right)^2 + \left(\frac{y}{a}\right)^2 = 1\tag{18}$$

Any point  $y_n$  on the elliptical frame of the dish with respect to  $x_n$ , can be given as,

$$y_n = \cos \beta \sqrt{b^2 - x_n^2} \tag{19}$$

As there are seven crossbars, they are equally distributed about the middle crossbar as discussed earlier. The distance between them is calculated as 0.665 m. The distance between the frame and the last crossbar is 0.655 m on either side. Fig. 7 summarize the details of coordinates of the intersection points of the crossbars with the elliptical rim of the Scheffler dish.

# Crossbar equations

The cutting planes of the crossbar when projected on the cutting plane of the reflector are obtained as straight lines. These lines for the crossbars are shown in Fig. 8. These cutting planes are also the ellipses inclined at  $-46.47^{\circ}$ . The axes ratio for each cutting plane is  $(a_C/b_C) = \cos 46.47$ . For middle crossbar  $C_4$ , the equation is given as,

$$y_{C_4}(x) = m_{C_4}x + q_{C_4} (20)$$

Here,  $m_{C_4}$  and  $q_{C_4}$  are the slope and y-intercept of the crossbar  $C_4$  respectively. The slope of the crossbar  $C_4$  is calculated as,

$$m_{C_4} = \tan\left(-46.47\right) = -1.0527\tag{21}$$

Now, the point  $C_{\rm f}$  also lies on this middle crossbar and it is the midpoint of line AB. Thus, its x-coordinate is the mean of x-coordinates of A and B which is 4.0565 m while its y-coordinate is, 2.3591 m. The y-intercept of the crossbar  $C_4$  is calculated as 6.6743 m.

Thus, the equation of crossbar  $C_4$  is obtained as,

$$y_{C_4}(x) = -1.0527x + 6.6743 (22)$$

The equations for the  $4^{th}$ ,  $5^{th}$  and  $6^{th}$  crossbars are calculated by adding 0.9655, 2(0.9655) and 3(0.9655) in the y-intercepts values of the above equation respectively.

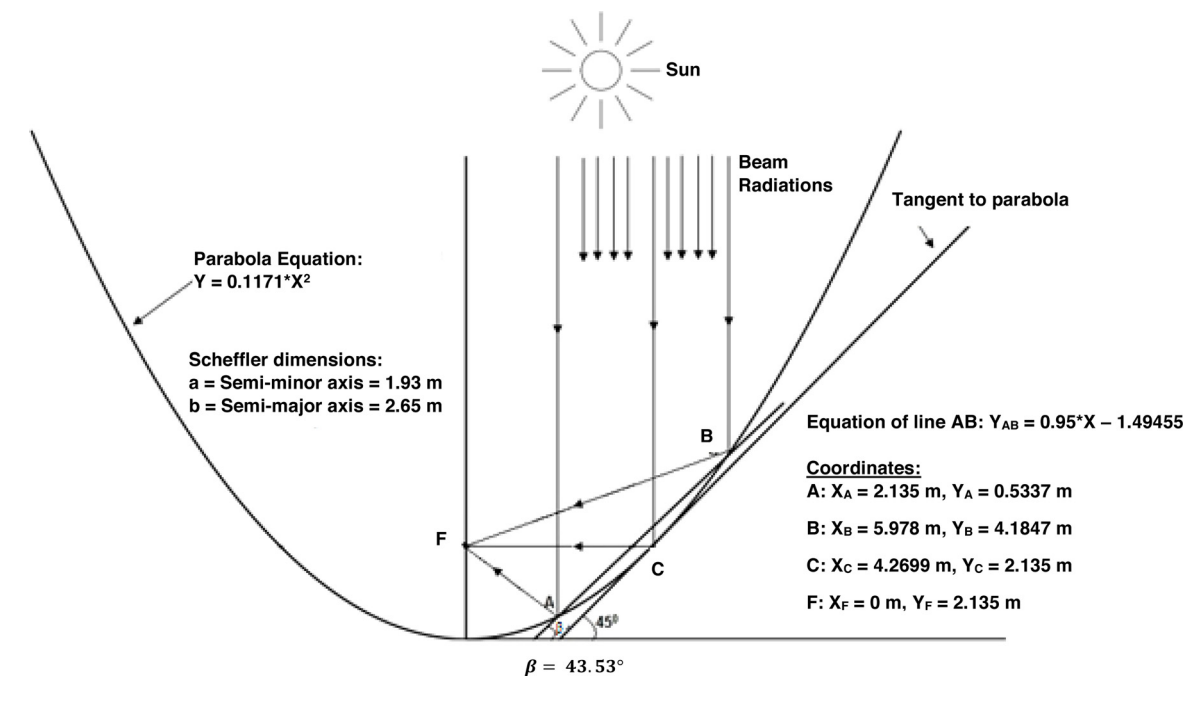
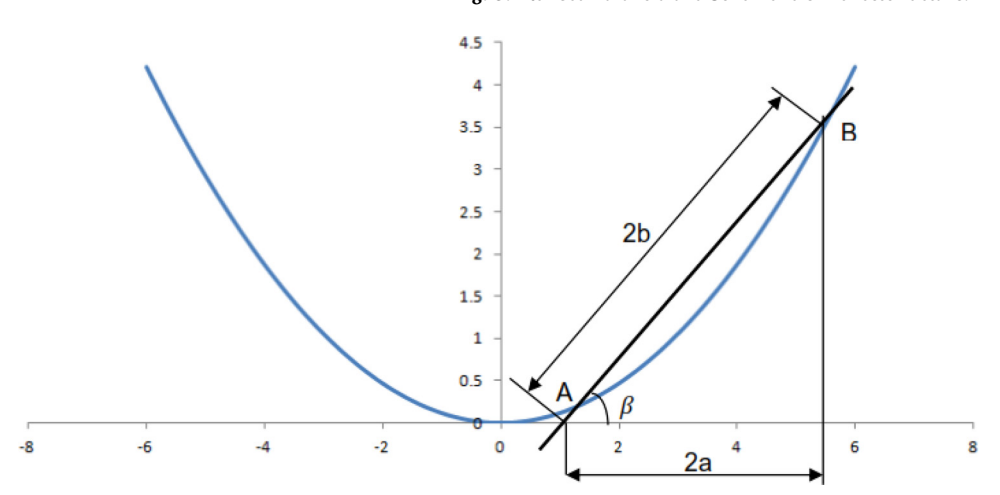


Fig. 5. Revised Parabola and Scheffler dish reflector details.



**Fig. 6.** Relation between the major and minor axis of Scheffler dish.

Similarly, the equations for  $3^{rd}$ ,  $2^{nd}$ , and  $1^{st}$  crossbars are calculated by subtracting 0.9655, 2(0.9655) and 3(0.9655) from the y-intercepts values of the above equation respectively.

The minor axis for  $n^{th}$  crossbar can be calculated from the following equation [11],

$$a_{Cn} = \sqrt{\left(\frac{m_{Cn}}{2m_p}\right)^2 + \frac{q_{Cn}}{m_p}} \tag{23}$$

Then the semi-major axis  $(b_{Cn})$  for the crossbar can be calculated from the following equation [11],

$$b_{Cn} = \frac{a_{Cn}}{\cos 46.47} \tag{24}$$

Table 3 summarizes the y-intercept, cutting plane equations, semi-major and semi-minor axes for all the crossbars.

Depths and arc lengths for different crossbars

The depth  $(\Delta_n)$ , the radius  $(R_n)$  and the arc length  $(b_{Cn})$  for each crossbar are calculated for the construction of the Scheffler parabola using the relations from [11],

The depth of reflector for n<sup>th</sup> crossbar is given as,

$$\Delta_n = \frac{a_{Cn} - \sqrt{a_{Cn}^2 - Y_n^2}}{\cos 46.47} \tag{25}$$

Fig. 9 shows the depth for the ellipse of the crossbar for the Scheffler reflector. From above Fig. 9, the radius  $(R_n)$  and half arc length  $(b_{Cn}/2)$  can be given as,

$$R_n^2 = \left(R_n - \Delta_n\right)^2 + Y_n^2 \tag{26}$$

Simplifying the above equation,

$$R_n = \frac{\sqrt{\Delta_n^2 + Y_n^2}}{2\Delta_n} \tag{27}$$

The half arc length is,

$$\frac{b_{Cn}}{2} = R_n \left(\frac{2\pi\beta_n}{360}\right) \tag{28}$$

Where,

$$\beta_n = \sin^{-1}\left(\frac{Y_n}{R_n}\right) \tag{29}$$

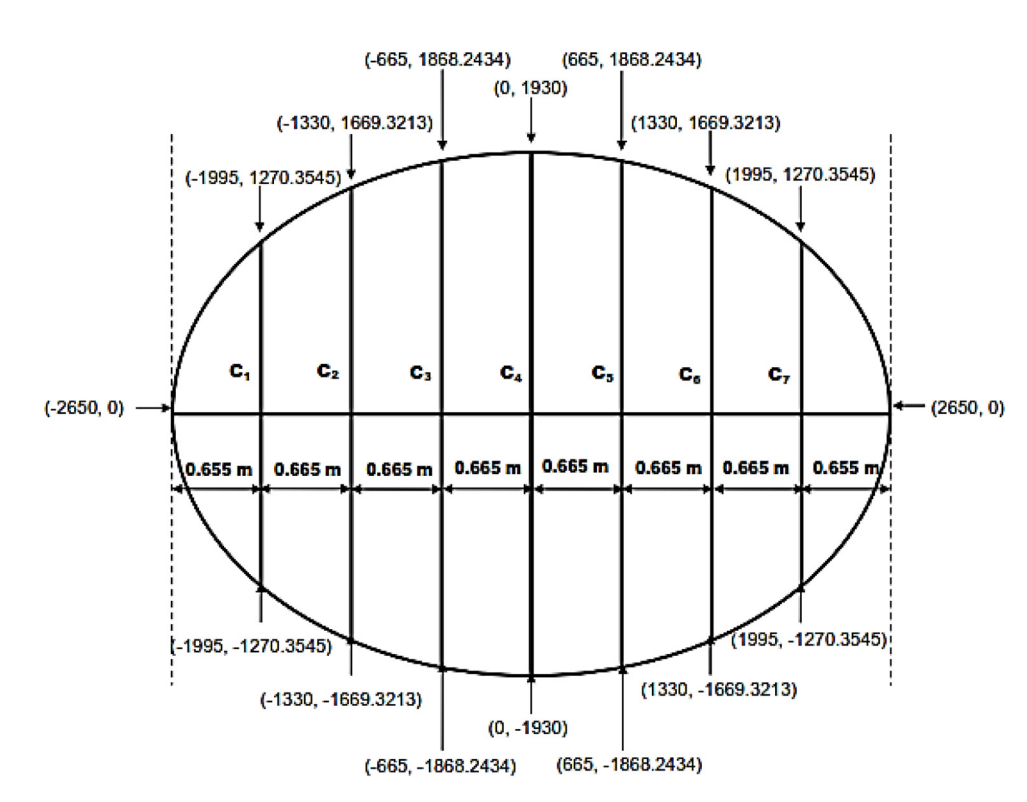


**Fig. 7.** Intersection points of seven crossbars for the elliptical frame of Scheffler dish.

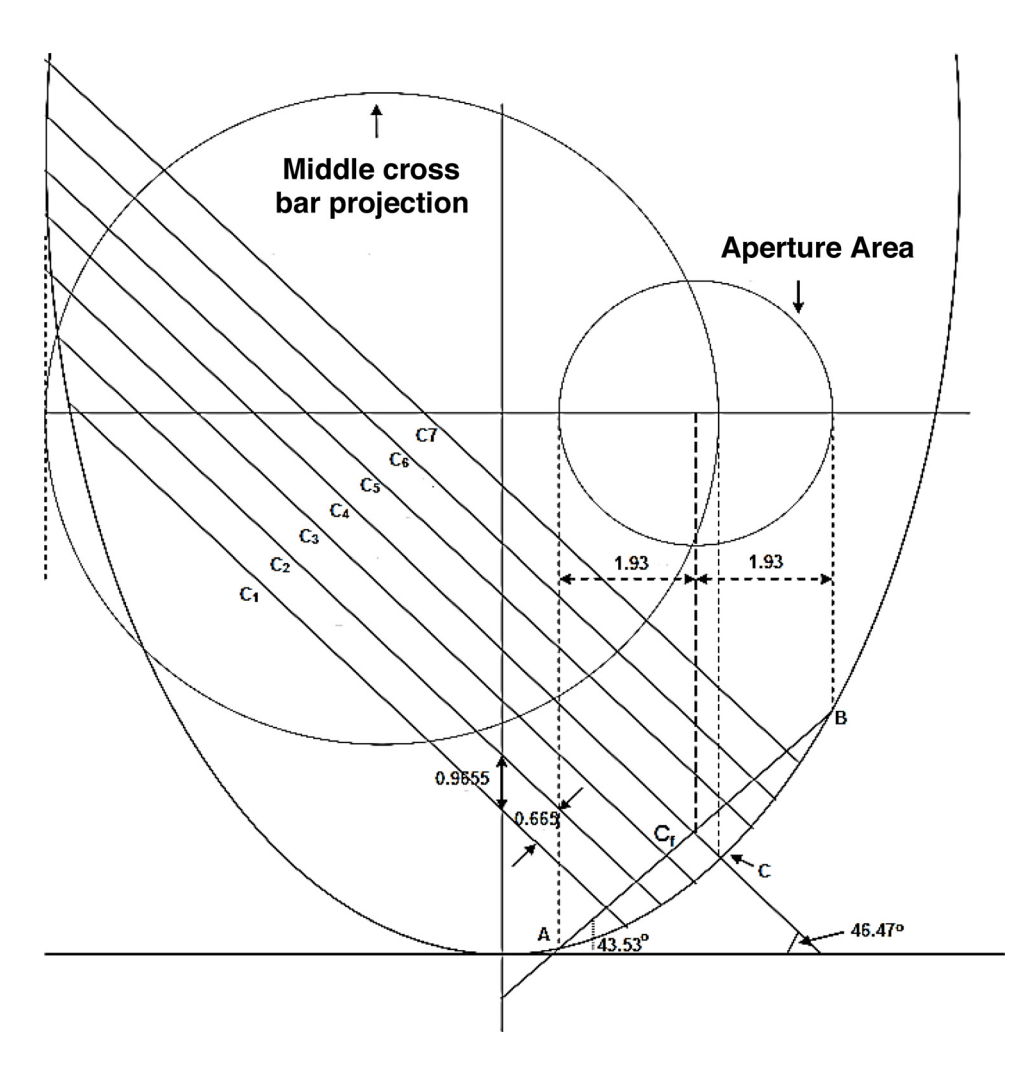


Fig. 8. Scheffler reflector with crossbar details.

**Table 3** y-intercept, cutting plane equations, semi-major and semi-minor axes for all the crossbars.

Crossbar No.	Y-intercept $q_{Cn}$	The equation of cutting plane of crossbars on XY plane	Semi-minor axis $(a_{Cn})$	Semi-major axis $(b_{Cn})$
1	3.7778	$\mathbf{y}_{C_1}(\mathbf{x}) = -1.0527\mathbf{x} + 3.7778$	8.5696	12.4425
2	4.7433	$\mathbf{y}_{C_2}(\mathbf{x}) = -1.0527\mathbf{x} + 4.7433$	9.0379	13.1225
3	5.7088	$\mathbf{y}_{C_3}(\mathbf{x}) = -1.0527\mathbf{x} + 5.7088$	9.4831	13.7689
4	6.6743	$\mathbf{y}_{C_A}(\mathbf{x}) = -1.0527\mathbf{x} + 6.6743$	9.9083	14.3863
5	7.6398	$\mathbf{y}_{C_s}(\mathbf{x}) = -1.0527\mathbf{x} + 7.6398$	10.3160	14.9782
6	8.6053	$\mathbf{y}_{C_6}(\mathbf{x}) = -1.0527\mathbf{x} + 8.6053$	10.7082	15.5477
7	9.5708	$\mathbf{y}_{C_7}(\mathbf{x}) = -1.0527\mathbf{x} + 9.5708$	11.0866	16.0970

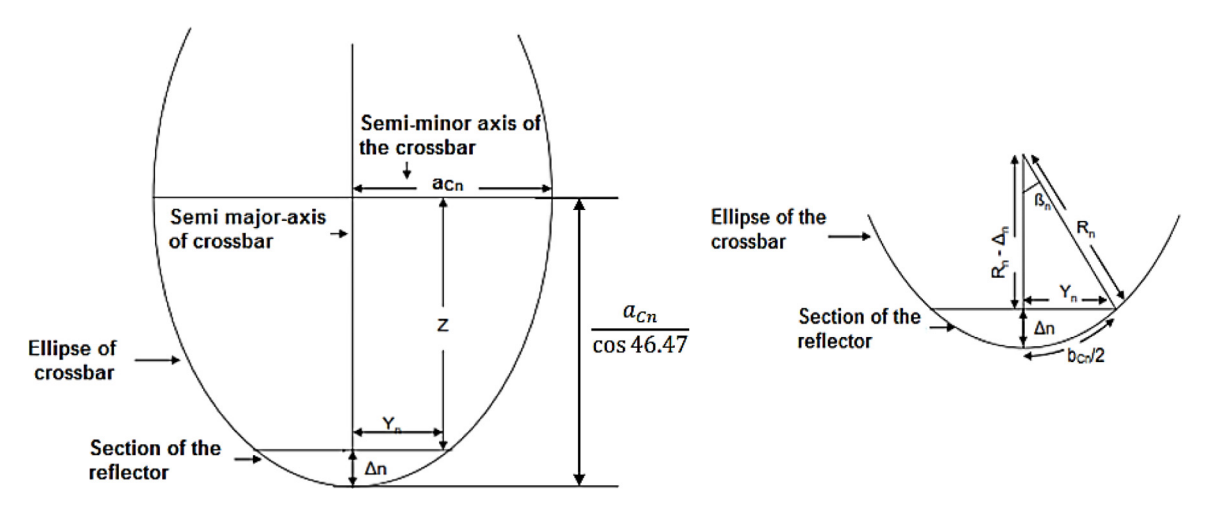


Fig. 9. Depth of crossbar ellipse [11].

**Table 4** Depth  $(\Delta_n)$ , radius  $(R_n)$  and arc length  $(b_{Cn})$  for each crossbar.

Crossbar no.	Y-coordinate Yn, m	$a_{Cn}$ (m)	$\Delta_n$ (m)	$R_n$ (m)	$\beta_n$	$b_{Cn}/2$ (m)	$b_{Cn}$ (m)
1	1.2709	8.5696	0.1376	4.6454	15.8774	1.2873	2.5746
2	1.6700	9.0379	0.2260	3.7289	26.6066	1.7316	3.4632
3	1.8690	9.4831	0.2701	3.4962	32.3165	1.9719	3.9439
4	1.9308	9.9083	0.2758	3.5360	33.0960	2.0425	4.0850
5	1.8690	10.316	0.2479	3.8030	29.4369	1.9539	3.9077
6	1.6700	10.7082	0.1902	4.4175	22.2126	1.7126	3.4252
7	1.2709	11.0866	0.1061	6.0092	12.2098	1.2806	2.5611

Table 4 summarizes calculated depth  $(\Delta_n)$ , radius  $(R_n)$  and arc length  $(b_{Cn})$  for each crossbar.

# Calculation of seasonal parabola equations and aperture area

The reflector needs to be adjusted with respect to the changes in the solar declination angle. This can be achieved using the telescopic clamp mechanism, as shown in Fig. 10, provided with the reflector.

By adjusting the inclination angle of the reflector equal to half of the change of the solar declination, the required shape of the parabola for any day of the year can be attained. To get the required shape of the parabola for any day, a fixed-point B with x-coordinate equal to x-coordinate of point  $C_f$  on the line AB is selected on the parabola curve.

This point acts as a common point for all the seasonal parabolas and also works as a pivotal point for attaining the required shape changes of the crossbars. Thus, the coordinates of point B are (4.0565, 1.9269).

The general equation of parabola for any day of the year can be given as,

$$D(x) = m_d x^2 + C_d \tag{30}$$

Here,  $\mathcal{C}_d$  is the y-intercept of the parabola curve. Now,

$$D'(x) = 2m_d x = tan\left(43.223 + \frac{\delta}{2}\right) \tag{31}$$

$$\delta = 23.45 \sin \left[ \frac{360}{365} (284 + n) \right] \tag{32}$$

Here, n is the day of the year and declination angle,  $\delta$  varies between  $-23.5^{\circ}$  to  $+23.5^{\circ}$  from December 21 to June 21 respectively [7,17].

The coordinates of a new set of points  $(x_s, y_s)$ , for any day of the year, can be obtained by using the following rotation matrix for rotating point B (4.0565, 1.9269) about the focus point F (0, 2.135).

$$(x_s, y_s) = (x, y) \begin{bmatrix} \cos \delta & \sin \delta \\ -\sin \delta & \cos \delta \end{bmatrix}$$
 (33)

Here,  $(x_s,y_s)$  indicates the coordinates of point B after rotation about focus F (0, 2.135). In summer, on June 21 reflector has to be rotated through 11.75 (+23.5/2) and in winter on Dec 21 it is to be rotated through -11.75 (-23.5/2). For summer the equation can be written as,

$$S(x) = m_s x^2 + C_s \tag{34}$$

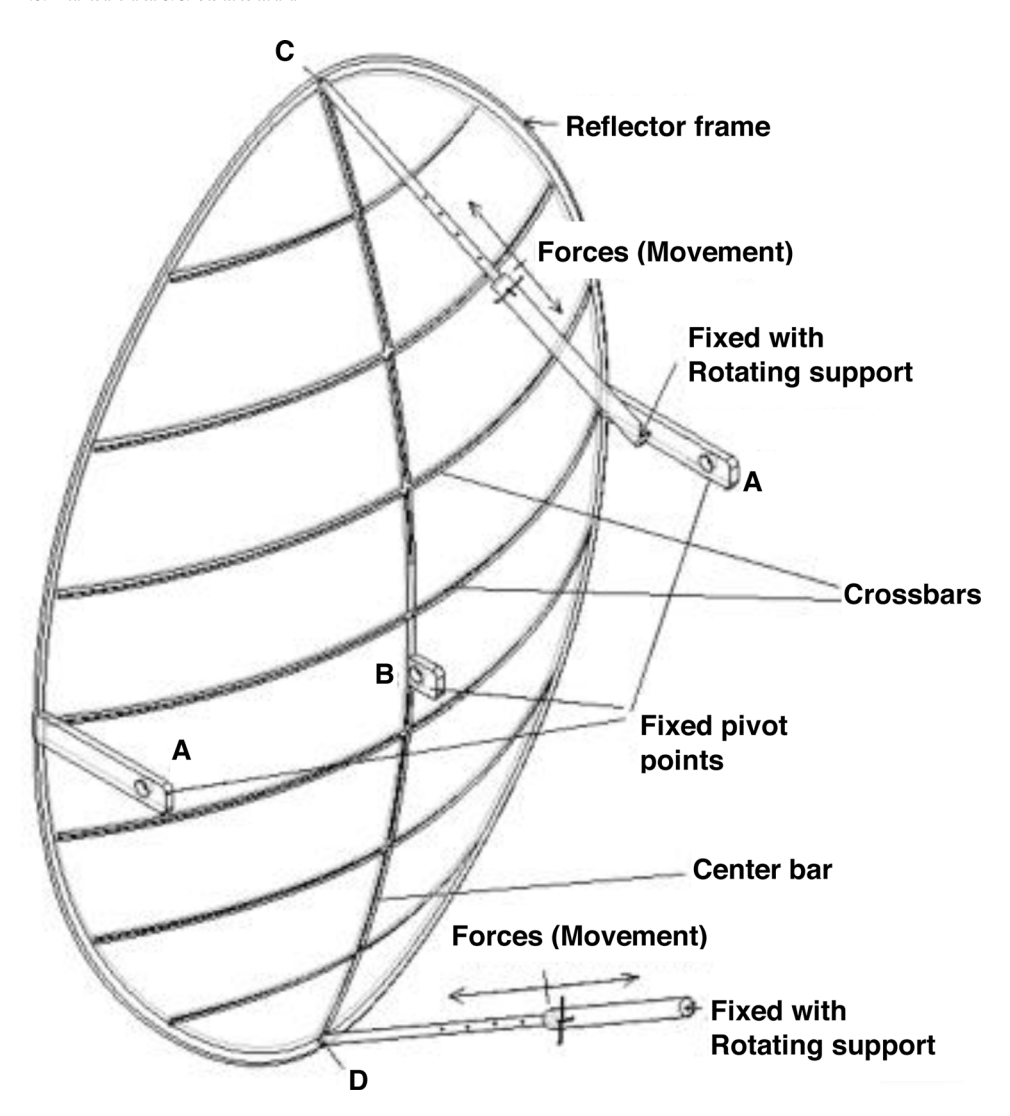
This is nothing but the slope of the parabola as discussed earlier which is given as,

$$S'(x) = 2m_s x = \tan\left(43.223 + \frac{\delta}{2}\right) \tag{35}$$

Substituting  $\delta = +11.75$  for summer in above equation. This indicates the extreme position in summer.

$$S'(x) = 2m_s x = 1.42676 (36)$$

**Fig. 10.** Telescopic clamp and the fixed-point details for Scheffler reflector [11].



For summer, at June 21,  $\delta = +23.5$ . As per the rule of the rotation matrix, as the point B is rotated about focus F (0, 2.135), the y-coordinate of F is initially subtracted from point B before solving the rotation matrix and then added again to the y-coordinate (i.e.,  $y_s$ ) obtained for the specific day, from the calculation.

$$(x_s, y_s) = (4.0565, 1.9269 - 2.135) \begin{bmatrix} cos23.5 & sin23.5 \\ -sin23.5 & cos23.5 \end{bmatrix}$$

Also,  $m_s=0.1875$  and  $C_s=0.8487$ . This defines the parabola equation for the summer season as,

$$y_s = 0.18758x_s^2 + 0.8487 (37)$$

Similarly, for winter at December 21,  $\delta$  = - 23.5. The equation of parabola for the winter season is obtained as,

$$y_w = 0.08415x_w^2 - 0.7865 (38)$$

The inclination of fixed-point B on parabola on June 21 and December 21 are  $55.28^{\circ}$  and  $31.78^{\circ}$ . These can be obtained by adding and subtracting  $11.75^{\circ}$  to the inclination angle of fixed-point B at the equinox  $(+43.53^{\circ})$ .

The summary of the seasonal parabola equations with the inclination angles at the equinox, summer (June 21) and winter (December 21) has been presented in the following Table 5.

Fig. 11 shows the three parabolas for summer, winter, and equinox. From Fig. 11 it can be observed that parabola shape is different in different seasons.

By comparing the different shapes of parabola, it can be observed that the parabola shape in summer is smaller and larger in winter. Thus, it can be concluded that for the same solar insolation, the energy collected by the Scheffler reflector is more in the winter season when compared to the summer season.

For calculating the parabola seasonal equations in the southern hemisphere, replace  $\delta$  in Eq. (33) by  $-\delta$ . Thus, the parabola equations for June 21 and December 21 will be the same as the parabola equations for December 21 and June 21 in the northern hemisphere.

Aperture area calculations for Scheffler concentrator

As discussed in earlier sections, the elliptical frame of the Scheffler reflector is not perpendicular to the beam radiations. It is inclined at  $(43.23 \pm \frac{\delta}{2})$  being the lateral part of the parabola. Thus, the available aperture area of the collector on any day of the year is given as,

$$A_s = A_f \cos\left(43.23 \pm \frac{\delta}{2}\right) \tag{39}$$

Here,  $A_s$  and  $A_f$  indicates the aperture area and reflector area for the Scheffler dish respectively.

The aperture area  $A_s$  is,

$$A_s = \pi ab \cos(43.23 \pm \delta/2) \tag{40}$$

The semi-major axis, b and semi-minor axis for the Scheffler is 2.65 m and 1.93 m respectively. Solar declination angle  $\delta$  varies from + 23.5°

 $\begin{tabular}{ll} \textbf{Table 5} \\ \textbf{Seasonal equations for 16} \ m^2 \ Scheffler \ Dish \ reflector in the northern hemisphere. \end{tabular}$ 

Season	Seasonal parabola equation	Y-intercept	Inclination angle $\beta$ for point B
Summer 21 June	$y_s = 0.18758x_s^2 + 0.8487$ $y_{C_2}(x) = -1.0527x + 4.7433$ $y_w = 0.08415x_w^2 - 0.7865$	0.8487	55.28°
Equinox (zero declination)		<b>0</b>	0°
Winter 21 December		-0.7865	31.78°

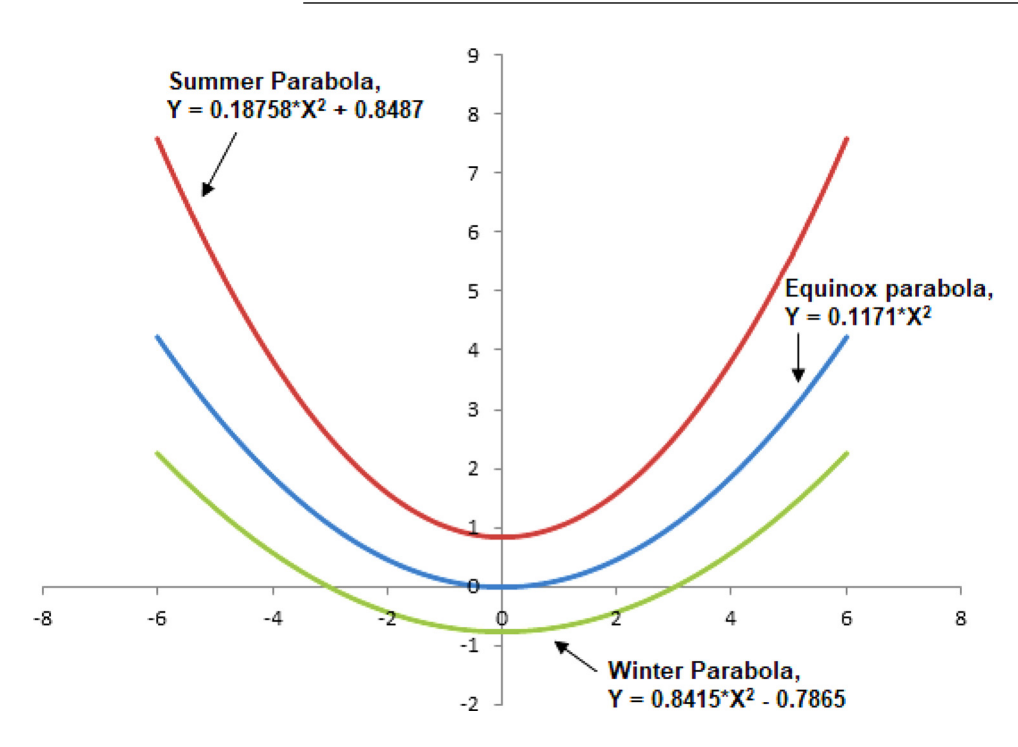


**Fig. 11.** Seasonal parabola details for standing type 16 m<sup>2</sup> Scheffler dish reflector for summer (June 21), Equinox and winter (December 21) in the northern hemisphere.

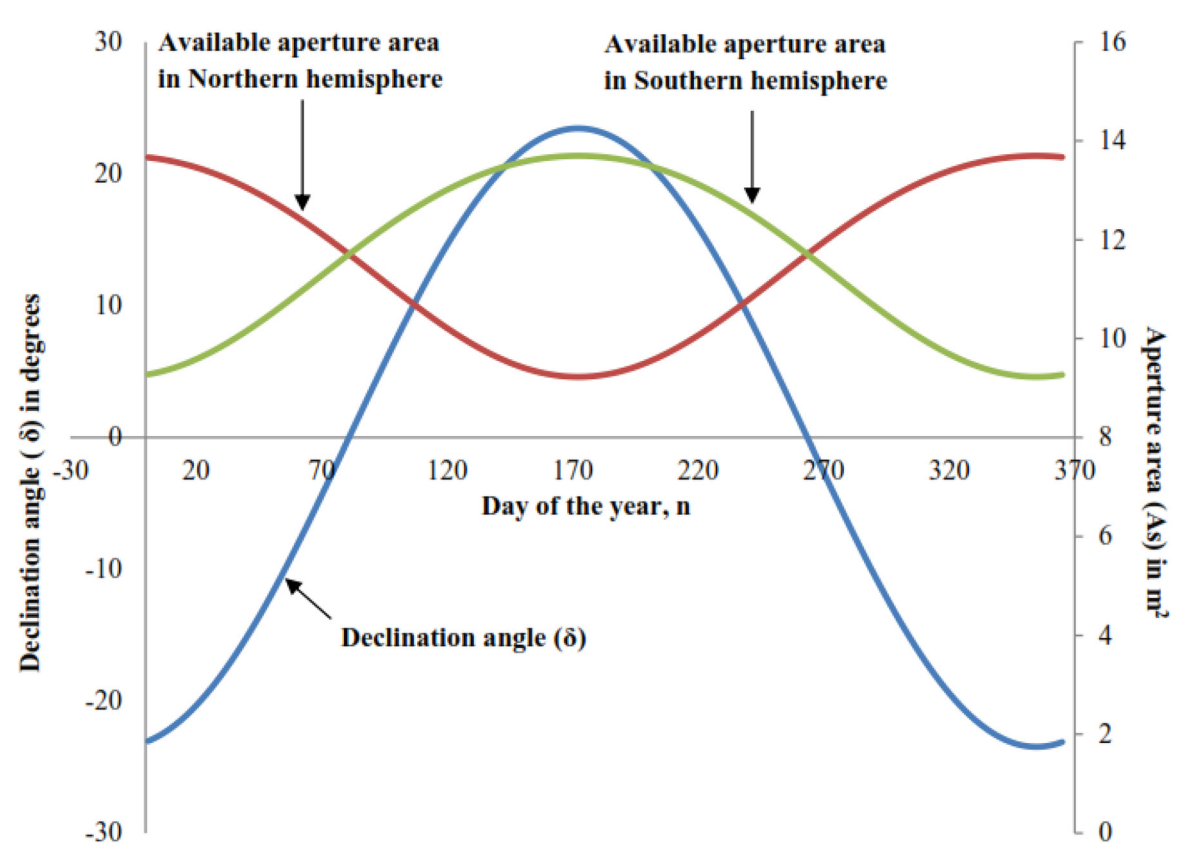


Fig. 12. Variation of aperture area and declination angle for the standing Scheffler reflector dish in the southern and northern hemisphere with days of the year.

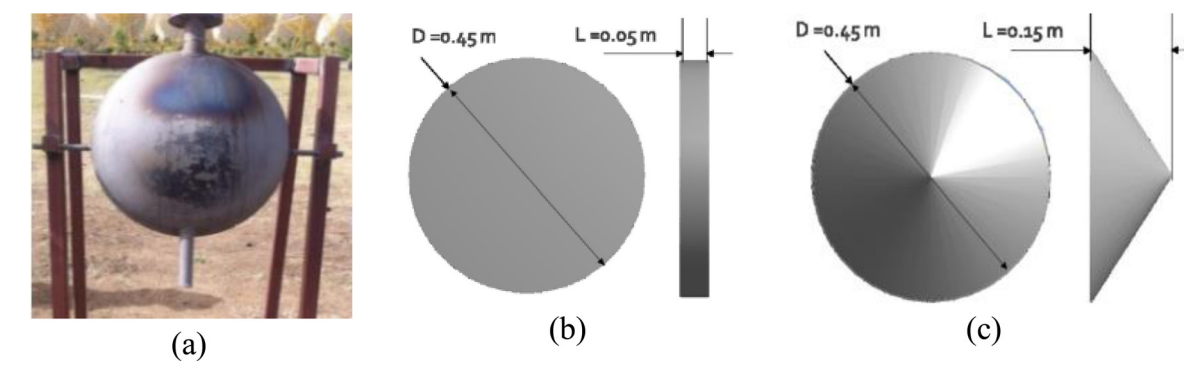


Fig. 13. Scheffler receivers (a) Dome type (b) Flat cylindrical type (c) Conical type [2].

on June 21 to - 23.5° on December 21. Fig. 12 shows the variation of aperture area and declination angle for the standing Scheffler reflector dish in the southern and northern hemispheres with days of the year.

From Fig. 12, it can be concluded that for the northern region hemisphere, the aperture area is lowest on June 21  $(9.3 \text{ m}^2)$  and highest on December 21  $(13.7 \text{ m}^2)$ . For the southern hemisphere, the aperture area is highest on June 21  $(13.7 \text{ m}^2)$  and lowest on December 21  $(9.3 \text{ m}^2)$ . At equinox (zero declination), the area is the same for both the hemisphere  $(11.7 \text{ m}^2)$ .

For the Scheffler concentrator, the beam radiations  $(I_{bn})$  are concentrated by the reflector and hence considered for the analysis. The diffused radiations  $(I_d)$  are not concentrated by the receiver and not available at the receiver, thus neglected.

#### Scheffler receiver and concentration ratio

The receiver kept at the focus of the Scheffler dish reflector receive the concentrated solar radiations from the dish. The working fluid flowing naturally at the inner surface of the receiver through the primary heat absorption circuit absorbs the heat energy from the concentrated solar radiations. The temperature at the receiver is highest in the complete primary heat absorption circuit and may reach above 200°C with a beam radiation range of 700 to 850 W/m² on a horizontal surface. The working fluid is generally received at the bottom of the receiver and moves in an upward direction when heated by concentrated solar radiation. The working fluid is further received in the header unit of the primary circuit. It is then circulated either through the process heat application for the direct heat utilization or inside the thermal storage system for the heat absorption. Thermic oils and water are generally used as the working fluids for heat absorption in the system.

Scheffler receiver is one of the key elements in the entire primary heat absorption circuit [37]. Different types of receivers are used in the applications. Few of the most commonly used receivers include,

- Flat cylindrical type receivers
- · Conical type receivers
- Dome type receivers

Flat cylindrical and dome type receivers are simple to manufacture as compared to conical types. Dome type receivers due to their shape can handle higher pressures when compared to flat cylindrical type receivers and thus mostly used with the Scheffler type concentrators. Fig. 13 below shows these three types of receivers.

## Size of the receiver

The shape or size and the capacity of the receiver is designed based on the optical and thermal analysis at the surface of the receiver. The image formed by the concentrated solar radiations at the focus of the Scheffler parabola decides the size of the receiver. Fig. 14 below shows

**Table 6**Total error calculation for Scheffler Parabolic reflector [19].

Type and Source	Effective Magnitude, $\sigma$ , mrad	$\sigma^2$
One-dimensional errors		
Structure	5	25
Tracking:SensorDrive non-uniformity	22	44
Receiver: Alignment, etc.	2	4
$(\sigma_{1-D})^2 = 37$		
$\sigma_{1-D} = 6.1 \text{ mrad}$		
Two-dimensional errors		
Mirror specular reflectance	0.5	0.25
Sun's width	2.8	7.84
$(\sigma_{2-D})^2 = 8.09$		
$\sigma_{2-D} = 2.8 \text{ mrad}$		

the image size for the reflection of non-parallel rays from a parabolic mirror.

The image analysis for the parabolic dish reflector is presented by [19] has been approximated for the Scheffler dish reflector for calculating the receiver size.

The width of the image formed at the focus of the parabolic dish considering different sources of errors: one dimensional and two dimensional is given as,

$$\Delta r = 2p \tan \left(\frac{n_i \sigma_{total}}{2}\right) \tag{40}$$

Here, p is the distance from the edge of the parabola to the focal point and  $\sigma_{total}$  is the total effective error at the focus due to both one dimensional and two-dimensional errors [19].  $n_i$  represents the number of standard deviations.

The one-dimensional errors consider the structural, tracking, receiver misalignment, etc. errors, while the two-dimensional errors include the sun's width and mirror specular errors. The total error including both one- and two-dimensional errors is calculated as shown in Table 6. The total error  $\sigma_{total}$  is calculated as,

$$\sigma_{total} = \sqrt{(\sigma_{1-D})^2 + (\sigma_{2-D})^2} = 6.7 \text{ mrad}$$
 (41)

The distance p for the Scheffler receiver is calculated as per the following Fig. 15 below,

The distance BF = p for the reflector is calculated by the following relation,

$$p = \sqrt{5.978^2 + 2.135^2} = 6.35 m \tag{42}$$

Considering the value of  $n_i$  equal to 6 ( $\pm$  3) for considering 99.73% of the total energy received at the receiver and value of  $\sigma_{total}$  and p calculated in Eqs. (41) and 42, the image size and hence the diameter of the receiver is calculated from Eq. (40) as,

$$\Delta r = 2p \tan\left(\frac{n_i \sigma_{total}}{2}\right) = 0.2553 m \tag{43}$$

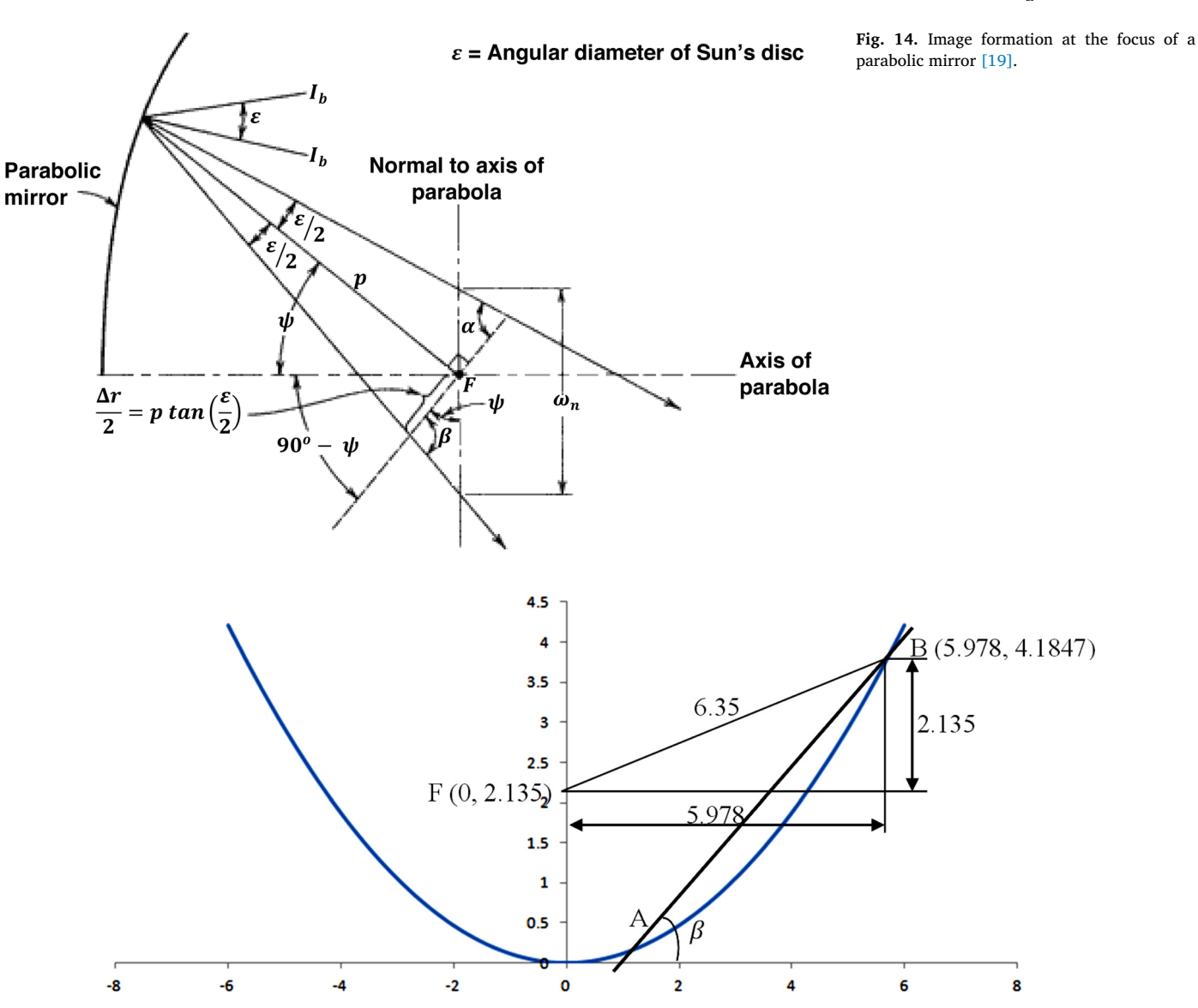


Fig. 15. Calculation of distance from the edge of the parabola to the focal point.

**Table 7** Receiver final dimensions.

Diameter (m)	0.5
Volume capacity, litre	15.5
Material	Boiler steel grade material, SS-304
Plate thickness, mm	5

Considering the actual errors in focusing, tracking, mirror alignment and errors in approximating the analysis for Scheffler the final diameter of the receiver is considered as 0.5 m. The total volume capacity for the dome type receiver is taken as 15.5 litres based on the thermal loss analysis. As the receiver is subjected to the highest temperature and pressure in the entire system, boiler grade material SS-306 with 5 mm thickness is selected for the receiver. The final dimensions of the receiver are summarized in Table 7 below,

## Concentration ratio

The Concentration Ratio (CR) is an important geometrical parameter for the solar concentrators. This ratio indicates the concentrator's ability to concentrate the solar energy [54]. Its value is constant and

fixed for a given concentrator after its manufacturing [54]. Higher the concentration ratio for a given concentrator, higher concentration and subsequently higher temperatures can be achieved at the focus of the concentrator. For the designed Scheffler receiver of diameter 0.5 m and Scheffler dish reflector area of 16 m $^2$  the concentration ratio based on the Scheffler reflector dish (SDR) area is given by the following equation

$$CR_{SDR} = \frac{Scheffler\ reflector\ area}{Receiver\ area} \tag{44}$$

 $CR_{SDR} = 81.48$ 

 $CR_{SDR}$  ratio provide the concentration ratio based on the standard Scheffler dish reflector size. It is constant for a given Scheffler concentrator with a given receiver and the reflector dish.

The Geometrical concentration ratio  $(CR_{geom})$  for a given concentrator is defined as the ratio of aperture area to the receiver area. As expected, for higher  $CR_{geom}$ , higher concentration and the temperatures will be achieved at the receiver. This ratio is based on the aperture area of the Scheffler concentrator and it is defined as,

$$CR_{geom} = \frac{Scheffler\ aperture\ area}{Receiver\ area}$$
 (45)

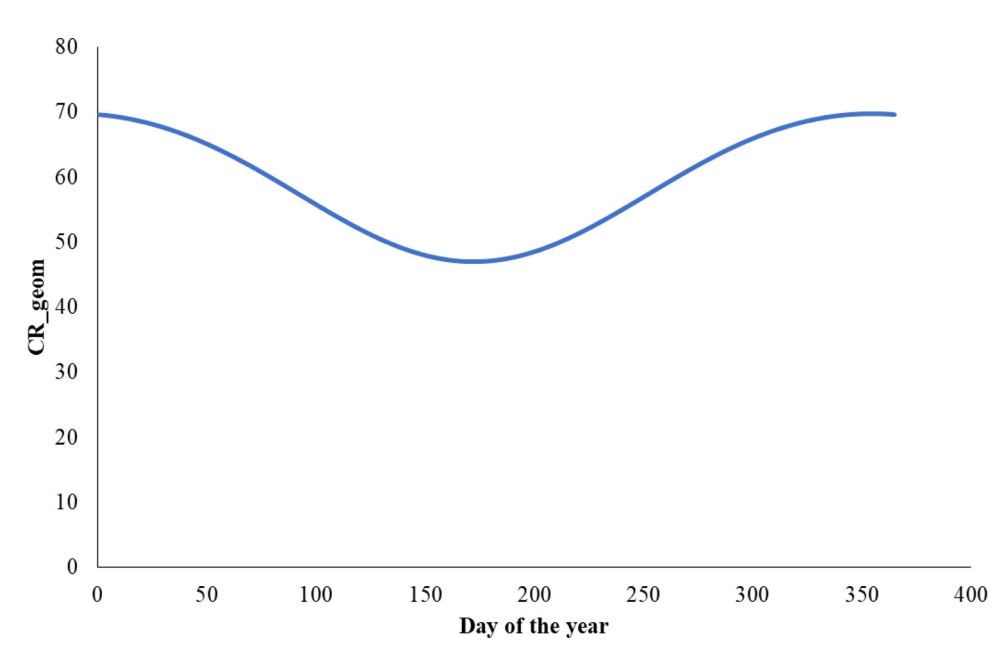


**Fig. 16.** Geometrical Concentration Ratio  $(CR_{geom})$  for Scheffler dish reflector of size 16 m<sup>2</sup> in the Northern hemisphere.

As shown in Fig. 12 the available aperture area for the Scheffler concentrator varies from maximum of 13.7 m² to minimum of 9.23 m² with the declination angle for the day at the given location. Thus, for the given Scheffler concentrator the geometrical concentration ratio also varies with the aperture area for the given day of the year. Fig. 16 below shows the variation of  $CR_{geom}$  with day of the year for the northern hemisphere. The highest and lowest  $CR_{geom}$  for the Scheffler dish of 16 m² size is 69.6 and 47.25 respectively. At equinox the available aperture area is 11.313 m². Thus,  $CR_{geom}$  at equinox for the Scheffler is calculated as 57.63.

The aperture area provides information about the actual area of the reflector that is visible to the solar rays. Thus, the geometrical concentration ratio is the most practical concentration ratio for the given receiver for all the practical engineering applications [54].

## Conclusion

This paper has presented a detailed stepwise design procedure for a 16 m<sup>2</sup> standing type Scheffler concentrator along with its dome-type receiver. Initially basic size Scheffler dish reflector has been designed, which is further resized to the desired size of 16 m2. The crossbar equations and elliptical frame calculations have also been discussed in detail for the 16 m<sup>2</sup> Scheffler reflector. The seasonal parabola equations are calculated with the variation in declination angle for the northern hemisphere. The aperture area calculated for the Scheffler reflector varies from 9.23 m<sup>2</sup> to 13.7 m<sup>2</sup>. Based on the image analysis at the receiver of the and thermal loss analysis, the diameter and the volume capacity for the stainless-steel receiver are calculated as 0.5 m and 15 liters respectively. The concentration ratio based on the reflector dish area and the geometrical concentration ratio at equinox for 16 m<sup>2</sup> Scheffler concentrator are estimated as 81.48 and 57.63 respectively. This design procedure can be suitably used for designing any size of Scheffler concentrator along with its dome type receiver.

# **Conflict of Interest**

All authors have participated in (a) conception and design, or analysis and interpretation of the data; (b) drafting the article or revising it critically for important intellectual content; and (c) approval of the final version. The authors have no affiliation with any organization with a direct or indirect financial interest in the subject matter discussed in the manuscript.

#### Acknowledgment

The research leading to these results has received Project Funding from The Research Council of the Sultanate of Oman under Research Grant No. BFP/RGP/EI/20/187. Authors would acknowledge the support and encouragement received from The Research Council as well as College of Engineering, National University of Science and Technology, Muscat Sultanate of Oman.

# References

- Abderrahman Mellalou, Abdelkader Outzourhit, Abdelaziz Bacaoui, Habiba Qaisari, Design methodologies of Scheffler Concentrators, in: 7th International Renewable and Sustainable Energy Conference (IRSEC), 2019, pp. 1–4.
- [2] Anita Nene, Ramachandran Arvind, S. Suyambazhahan, Effect of wind flow on convective heat losses from Scheffler solar concentrator receivers, J. Instit. Eng. (India) 100 (5) (2018) 737–745.
- [3] Anil Kumar, Experimental investigation of a Scheffler reflector for the medium temperature applications, J. Therm. Eng. 7 (5) (2021) 1302–1314, doi:10.18186/thermal 978197
- [4] Anil Kumar, Om Prakash, Ajay Kumar Kaviti, A comprehensive review of Scheffler solar collector, Renewable Sustainable Energy Rev. 77 (2017) 890–898, doi:10.1016/j.rser.2017.03.044.
- [5] Desireddy Shashidhar Reddy, Mohd.Kaleem Khan, Md.Zeeshan Alam, Haroon Rashid, Design charts for Scheffler reflector, Sol. Energy 163 (2018) 104–112.
- [6] Y. Devarajan, B. Nagappan, G. Subbiah, E. Kariappan, Experimental investigation on solar-powered ejector refrigeration system integrated with different concentrators, Environ. Sci. Pollution Res. 28 (13) (2021) 16298–16307, doi:10.1007/s11356-020-12248-z.
- [7] J.A. Duffie, W.A. Beckman, Solar Engineering of Thermal Processes, Wiley, 2013 fourth edition.
- [8] Hitesh Panchal, Jay Patel, Kiran Parmar, Mayank Patel, Different applications of Scheffler reflector for renewable energy: a comprehensive review, Int. J. Ambient Energy 41 (6) (2020) 716–728, doi:10.1080/01430750.2018.1472655.
- [9] Islam Q.U., Khozaei F., The Review of Studies on Scheffler Solar Reflectors. In: Dawn S., Balas V., Esposito A., Gope S., Intelligent Techniques and Applications in Science and Technology. ICIMSAT 2019. Learning and Analytics in Intelligent Systems, vol 12. Springer, Cham. Switzerland, 12 (2020), 589–595, ISBN 978-3-030-42363-6. doi:10.1007/978-3-030-42363-6.69.
- [10] Kajal J. Sareria, Jigar K. Andharia, Piyush B. Vanzara, Subarna Maiti, A comprehensive review of design parameters, thermal performance assessment, and medium temperature solar thermal applications of Scheffler concentrator, Cleaner Eng. Technol. 6 (2022) 100366 1-8.
- [11] A. Munir, O. Hensel, W. Scheffler, Design principle and calculations of a Scheffler fixed focus concentrator for medium temperature applications, Sol. Energy 84 (2010) 1490–1502.
- [12] A. Munir, Design, Development and Modelling of a Solar Distillation System For the Processing of Medicinal and Aromatic plants. PhD Thesis, Institute of Agricultural Engineering, University of Kassel, Germany, 2010.
- [13] A. Munir, O. Hensel, W. Scheffler, H. Hoedt, W. Amjad, A. Ghafoor, Design, development and experimental results of a solar distillery for the essential oils extraction from medicinal and aromatic plants, Sol. Energy 108 (2014) 548–559.

- [14] Parimal Bhambare, M.C. Majumder, C.V. Sudhir, Solar thermal desalination: a s ust ain able alternative for Sultanate of Oman, Int. J. Renew. Energy Res. 8 (2018) 733–751.
- [15] Parimal Bhambare, M.C. Majumder, C.V. Sudhir, Decentralized stand-alone Multi Effect Desalination (MED) system using fixed focus type Scheffler concentrator for the remote and arid rural regions of Sultanate of Oman, IOP Conf. Ser. 376 (2018) 012006. doi:10.1088/1757-899X/376/1/012006.
- [16] Simone Alberti, Analysis and Optimization of the Scheffler Solar Concentrator. MTech Thesis, California Polytechnic State University, 2014.
- $\hbox{\tt [17]} \ \ \text{S.P. Sukhatme, J.K. Nayak, Solar Energy, Tata McGraw Hill, 2008 Third Edition.}$
- [18] Vikrant Kamboj , Himanshu Agrawal , Anish Malan , Avadhesh Yadav , Thermal performance of t h e steam boiler based on Scheffl er solar concentrator for domestic application: experimental investigation, Austr. J. Mech. Eng. (2019) 1–11, doi:10.1080/14484846.2019.1656148.
- [19] William Stine, Michael Geyer, Solar Energy Systems Design (Power From The Sun), John Wiley and Sons (1986) https://www.powerfromthesun.net/index.html.
- [20] Wolfgang Scheffler, S. Bruecke, G. von Werdenbergstr, Introduction to the revolutionary design of Scheffler reflectors, in: Solar Cookers and Food Processing International Conference, 2006, pp. 12–16. Granada, Spain.
- [21] P. Suresh, M.D. Irfan Ali, P. GovindRao, Ramesh Rudrapati, Performance analysis of an Injera baking machine by using solar energy, Mater. Today: Proc. 56 (6) (2022) 3285–3293.
- [22] Gadhia Deepak, Parabolic solar concentrators for cooking, food processing and other applications, in: Korean Society for Renewable Energy: Proceedings of the Conference, 2006, pp. 165–167.
- [23] Katlego Lentswe, Ashmore Mawire, Prince Owusu, Adedamola Shobo, A review of parabolic solar cookers with thermal energy storage, Heliyon 7 (10) (2021) 1-16.
- [24] Christoph Müller, Solar community bakeries on the Argentinean Altiplano, International Solar Food Processing Conference, 2009 Indore, India.
- [25] Gregor Schapers, Agave syrup production a sweet tradition goes solar, International Solar Food Processing Conference, 2009 Indore, India.
- [26] Iqra Ayub , Anjum Munir , Abdul Ghafoor , Waseem Amjad , Muhammad salman nasser, solar thermal application for decentralized food baking using Scheffler reflector technology , J. Sol. E nergy Eng. 140 (2018) 1–9.
- [27] R.J. Patil, G.K. Awari, M.P. Singh, Experimental analysis of Scheffler reflector water heater, Therm. Sci. 15 (3) (2011) 599–604.
- [28] F.A. Nouh, S. Saidi, Y. Janah, L. Mandi, A. Kettab, Experimental study of a distillation unit by the use of a Sheffler solar Parabola, Algerian J. Environ. Sci. Technol. 3 (1) (2017) 342–347.
- [29] B. Joshi, R. Khairnar, Using scheffler cooker for solar cooking and other applications, Conf. Emerg. Trends Solar Technol. (2013) 15–25.
- [30] C.V. Sudhir, S. Feroz, Potential of 16 m<sup>2</sup> solar Scheffler reflectors for thermal applications experimental investigation, Int. J. Adv. Sci. Eng. Technol. 4 (2) (2016) 42–46.
- [31] U.B.R. Ragula, S. Devanathan, R. Mohan, Solar based lemon grass essential oil distillation for sustainability and livelihood in tribal community, IEEE Global Humanitarian Technol. Conf. (GHTC) (2016) 738–744.
- [32] S. Indora, T.C. Kandpal, Institutional and community solar cooking in India using SK-23 and Scheffler solar cookers: a financial appraisal, Renew. Energy 120 (2018) 501–511.
- [33] S. Indora, T.C. Kandpal, Financial appraisal of using Scheffler dish for steam based institutional solar cooking in India, Renew. Energy 135 (2019) 1400–1411.
- [34] A.C. Kashyap, J.P. Kesari, Feasible study of a solar crematorium in India, Int. J. Res. Scient. Innovat. 1 (IV) (2014) 1–9.

- [35] Vishal R. Dafle\*, Prof. N.N.Shinde, Design, development & performance evaluation of concentrating monoaxial Scheffler technology for water heating and low temperature industrial steam application, Int. J. Eng. Res. Appl. 2 (6) (2012) 848–852.
- [36] Lu Wang, Zhongxian Yuan, Yan Zhao, Zhanquan Guo, in: Review On Development of Small Point-Focusing Solar Concentrators, 28, 2019, pp. 929–947.
- [37] Dnyaneshwar Malwad, Vinod Tungikar, Experimental performance analysis of an improved receiver for Scheffler solar concentrator, SN Appl. Sci. 2 (1992) 2020.
- [38] Ajay Chandak, Sunil Somani, Industrial Oven powered with a pair of Scheffler solar collectors, Proc. Solar World Congr. (2011) 1357–1364 Kassel, Germany.
- [39] Erick Alfred Dib, Luanda Gimeno Marques, Renan Tavares Figueiredo, Flávio Augusto Sanzovo Fiorelli, Technical analysis of an oven with coupled receiver for Scheffler solar concentrator tested under cloudy weather conditions, Acta Scientiarum Technol. 42 (2020).
- [40] Miguel Hadzich, François Veynandt, Julien Delcol, Luis Miguel Hadzich, Juan Pablo Pérez, Sandra Vergara, Design of a Solar Coffee Roaster for Rural Areas, Energy Procedia 57 (2014) 3215–3224.
- [41] Swati Bhasme, A.G. Thosar, Performance Analysis of Scheffler Reflector used for Solar Dry Cleaning, Int. J. Eng. Innovat. Res. 4 (4) (2015) 640–644.
- [42] Desireddy Shashidhar Reddy, Mohd.Kaleem Khan, Stationary point focus solar concentrators—A review, Int. J. Energy Res. 46 (5) (2022) 5678–5702.
- [43] E. Assareh, M. Assareh, S.M. Alirahmi, M. Shayegh, F. Wang, M. Behrang, X. Wang, Thermodynamic assessment of a cogeneration system with CSP Driven-Brayton and Rankine cycles for electric power and hydrogen production in the framework of the energy and water nexus. Energy Nexus 5 (2022) 100031.
- [44] Z. Li, X. Xu, X. Sheng, P. Lin, J. Tang, L. Pan, Y. Yamauchi, Solar-powered sustainable water production: state-of-the-art technologies for sunlight-energy-water nexus, ACS Nano 15 (8) (2021) 12535–12566.
- [45] M.A. Tony, Nexus approach: ZSM-12 derived from industrial waste into microencapsulated in organic wax for solar energy storage system, Energy Sources Part A (2021) 1–19.
- [46] Tabanja, A., Solar energy in the food-water-energy nexus, a case study on solar water pumps for irrigation in Punjab, Pakistan (Doctoral dissertation), (2021).
- [47] J. Yu, Y.M. Tang, K.Y. Chau, R. Nazar, S. Ali, W. Iqbal, Role of solar-based renewable energy in mitigating CO2 emissions: evidence from quantile-on-quantile estimation, Ren ew. Energy 182 (2022) 216–226.
- [48] M.H. Shahverdian , A. Sohani , H. Sayyaadi , Water-energy nexus performance investigation of water flow cooling as a clean way to enhance the productivity of solar photovoltaic modules , J. Clea n. Pro d. 312 (2021) 127641.
- [49] G.F. Sargentis, P. Siamparina, G.K. Sakki, A. Efstratiadis, M. Chiotinis, D. Koutsoyiannis, in: Agricultural Land or Photovoltaic Parks? The Water-Energy-Food Nexus and Land Development Perspectives in the Thessaly Plain, 13, 2021, p. 8935. Greece, Sustainability.
- [50] J. Chenoweth , R.A. Al-Masri , The impact of adopting a water-energy nexus approach in Jordan on transboundary management , Env iron . Sc i. Policy 118 (2021) 49–55
- [51] A. Panagopoulos, Water-energy nexus: desalination technologies and renewable energy sources, Environ. Sci. Pollution Res. 28 (17) (2021) 21009–21022.
- [52] J.P.E. Dinkel, Texas Sun: A Fixed Effects Panel Approach to the Solar Energy-Economic Growth Nexus At the County Level, Georgetown University, 2021.
- [53] Shireesh B. Kedare, Nishith B. Desai, Solar Thermal Process Heat, Encyclopedia of Sustainable Technologies, edited by Martin A. Abraham, 367–376, Elsevier, 2017.
- [54] Hongfei Zheng, Solar Energy Utilization and Its Collection Devices, Solar Energy Desalination Technology, edited by Hongfei Zheng, 47–171, Elsevier, 2017.